

ED⁴: Explicit Data-level Debiasing for Deepfake Detection

Jikang Cheng^{1*}, Ying Zhang², Qin Zou¹, Zhiyuan Yan³, Chao Liang¹,
Zhongyuan Wang^{1†}, Chen Li²

¹School of Computer Science, Wuhan University

²WeChat, Tencent

³The Chinese University of Hong Kong, Shenzhen (CUHK-Shenzhen)

Abstract

Learning intrinsic bias from limited data has been considered the main reason for the failure of deepfake detection with generalizability. Apart from the discovered content and specific-forgery bias, we reveal a novel *spatial bias*, where detectors inertly anticipate observing structural forgery clues appearing at the image center, also can lead to the poor generalization of existing methods. We present ED⁴, a simple and effective strategy, to address aforementioned biases *explicitly at the data level* in a unified framework rather than implicit disentanglement via network design. In particular, we develop ClockMix to produce facial structure preserved mixtures with arbitrary samples, which allows the detector to learn from an exponentially extended data distribution with much more diverse identities, backgrounds, local manipulation traces, and the co-occurrence of multiple forgery artifacts. We further propose the Adversarial Spatial Consistency Module (AdvSCM) to prevent extracting features with spatial bias, which adversarially generates spatial-inconsistent images and constrains their extracted feature to be consistent. As a model-agnostic debiasing strategy, ED⁴ is *plug-and-play*: it can be integrated with various deepfake detectors to obtain significant benefits. We conduct extensive experiments to demonstrate its effectiveness and superiority over existing deepfake detection approaches.

Introduction

The growing threats posed by deepfake technology in social media have heightened the necessity of detecting malicious deepfake content. Hence, deepfake detection technology attracts increasing attention from the research community. Most deepfake detectors perform promisingly when dealing with in-dataset images. However, their effectiveness faces significant challenges when transferred to unseen data distribution, which restricts their ability in practical usage.

To improve the generalization ability, existing deepfake detectors make attempts from multiple aspects (Nguyen, Yamagishi, and Echizen 2019; Haliassos et al. 2021; Huang et al. 2023; Liang, Shi, and Deng 2022; Yan et al. 2023a). Among them, methods targeted at removing the model bias hold the view that, deepfake detectors could easily learn the biased information to categorize input data,

*Work done during an internship at WeChat

†Corresponding Author

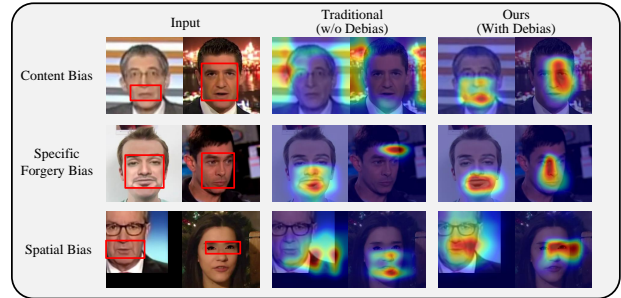


Figure 1: Illustration of different biases in deepfake detection. Two inputs for specific-forgery bias are in-dataset and cross-dataset, respectively. The red rectangle indicates the region containing the ground-truth forgery traces. We discover that the traditional detector may mistakenly focus on **Content Bias**: The striking background without considering the possible forgery artifacts presented in the faces. **Specific-Forgery Bias**: Specific in-dataset artifacts. **Spatial Bias**: Structural forgery clues at the image center despite the faces being shifted or locally manipulated.

rather than digging the intrinsic forgery evidence. Liang *et al.* (Liang, Shi, and Deng 2022) demonstrate that detectors erroneously learn the identity and background information, which can be referred to as content bias. Then, they design an encoder-decoder network, attempting to achieve feature disentanglement through implicit network constraints. Yan *et al.* (Yan et al. 2023a) contend that detectors tend to focus on the forgery artifacts related to one specific manipulation method, thereby overlooking common forgery artifacts. To address such specific-forgery bias, they also adopt a similar encoder-decoder network to disentangle common forgery features. With inspiring observations and analyses, these methods struggled to **implicitly** separate the generalizable forgery features from bias with an encoder-decoder network, which is **non-intuitive and insufficient to guarantee successful disentanglement**. Broadly speaking, the fake synthesis methods can be considered as a way of removing the model bias by creating new fake images. However, their performance is hindered by the limitation in mixing identities (Shiohara and Yamasaki 2022; Dong et al. 2023), fake regions (Chen et al. 2022), or blend types (Li et al. 2020a).

Apart from the *content bias* and *specific-forgery bias*, as shown in Fig. 1, we first reveal a novel model bias that has been previously underestimated, which we term *spatial bias*. Specifically, we notice that detectors usually expect to observe structural forgery clues at the image center, regardless of the actual facial location or the existence of local forgery artifacts. Therefore, the learned forgery information during training is oversimplified and the model sensitivity to forgery artifacts is severely compromised. Moreover, spatial bias can significantly undermine the robustness of the detector by posing challenges against spatial deviation, which commonly occurs in face detection and preprocessing.

In this paper, we propose Explicit Data-level Debiasing for Deepfake Detection (ED⁴) aiming to address the aforementioned three biases in a unified framework. Specifically, we introduce two effective modules to remove the model bias in a hybrid manner: ClockMix, and Adversarial Spatial Consistency Module (AdvSCM). ClockMix aims to address the content and specific-forgery biases via the clockwise mixing of different images. It takes multiple images with arbitrary faces as input, and then performs sector-based mosaicing centered on the face, to obtain a mixture containing different backgrounds, identities, and forgery artifacts. Different from existing mixing strategies, ClockMix is carefully designed for face forgery detection with high flexibility and surprising effectiveness. Then, we propose AdvSCM to tackle spatial bias. Specifically, we introduce an adversarial generator to produce shuffled images with larger spatial inconsistency. Subsequently, we enforce the detector to learn consistent forgery feature representations of images with distinct spatial-inconsistent versions. By introducing AdvSCM, the deepfake detector is forced to ignore spatial deviations and pay more attention to informative local regions, thus gaining stronger discriminant power in identifying subtle forgery patterns rather than inertly anticipating the observation of structural forgery clues at image centers.

By explicitly removing the model bias at the data level, ED⁴ is a superior alternative to the implicit disentanglement achieved by designing networks (Liang, Shi, and Deng 2022; Yan et al. 2023a), as well as to traditional fake synthesis approaches (Chen et al. 2022; Dong et al. 2023; Li et al. 2020a; Shiohara and Yamasaki 2022). The advantages could be summarized as:

- ED⁴ feeds the network with images covering more varied identities, backgrounds, forgery patterns, and spatial distributions, which can intuitively improve the network generalization with the **increased data diversity**.
- ED⁴ achieves stronger data augmentation by mosaicing arbitrary face images, **with no limitation** in image labels, paired identities, or fake regions.
- ED⁴ is model-agnostic and can be easily applied as a **plug-and-play** module to improve the deepfake detection methods, without introducing computation overhead during inference.

Related Works

Deepfake Detection Deepfake detection aims to classify the authority of an input image, which may be forged by

deepfake manipulations. Some approaches focus primarily on specific facial representations, such as lips movement (Haliassos et al. 2021) and action unit consistency (Bai et al. 2023). Meanwhile, various studies are dedicated to developing optimal neural network structures to improve detection performance, such as MesoNet (Afchar et al. 2018), Xception (Chollet 2017), and CapsuleNet (Nguyen, Yamagishi, and Echizen 2019). In the frequency domain, SPSL (Liu et al. 2021) and SRM (Luo et al. 2021) introduce the phase spectrum and high-frequency noises to enhance the forgery information for training. These methods focus on identifying specific vulnerabilities inherent in Deepfake methods, achieving significant success in detecting fake images that exhibit these specific vulnerabilities.

Owing to the limited data variations, certain specific data characteristics may be exclusively found within the data associated with a particular label. Subsequently, the detector may take a shortcut by solely learning the correlation between certain characteristics and the label, neglecting to achieve an in-depth comprehension of forgery features. We refer to this inert mapping as model bias. Dong *et al.* (Dong et al. 2023) and Huang *et al.* (Huang et al. 2023) posit that the target face identity used during face swapping remains in the fake face, leading to implicit identity leakage. Liang *et al.* (Liang, Shi, and Deng 2022) recognize the issue of content bias in deepfake detection, suggesting that networks might mistakenly treat certain identities or backgrounds as either Fake or Real based on learned biases from the training data without learning the actual forgery information. Subsequently, they design an encoder-decoder network to implicitly disentangle the content bias, attempting to obtain a forgery-only feature for detection. Similarly, specific-forgery bias refers to detectors overfitting method-specific-forgery artifacts, thereby exhibiting a lack of sensitivity to common forgery and demonstrating limited generalizability. UCF (Yan et al. 2023a) utilizes indirect constraints and network design to implicitly disentangle common forgery features from specific features, guiding the learning toward generalized forgery information.

While these methods demonstrate the significance of content and specific-forgery biases, the implicit disentanglement achieved by the encoder-decoder network design appeared overly complex and indirect. Namely, the components for decoding are redundant during inference and are limited to indirectly constrain the encoder for the disentanglement during training.

Data Augmentation and Synthesis for Deepfake Detection Data augmentation is widely employed during the training of neural networks to enhance the generalizability of the model, which enriches data diversity by implementing spatial transformations to the training samples. Various traditional data augmentation methods have been demonstrated to exhibit significant impacts on the generalizability of deepfake detectors. For instance, Liang *et al.* (Liang, Shi, and Deng 2022) attempts to incorporate the feature-level Mixup, while Wang *et al.* (Wang and Deng 2021) designed a specific version of random erasing (Zhong et al. 2020) based on attention for deepfake detection. DCL (Sun et al.

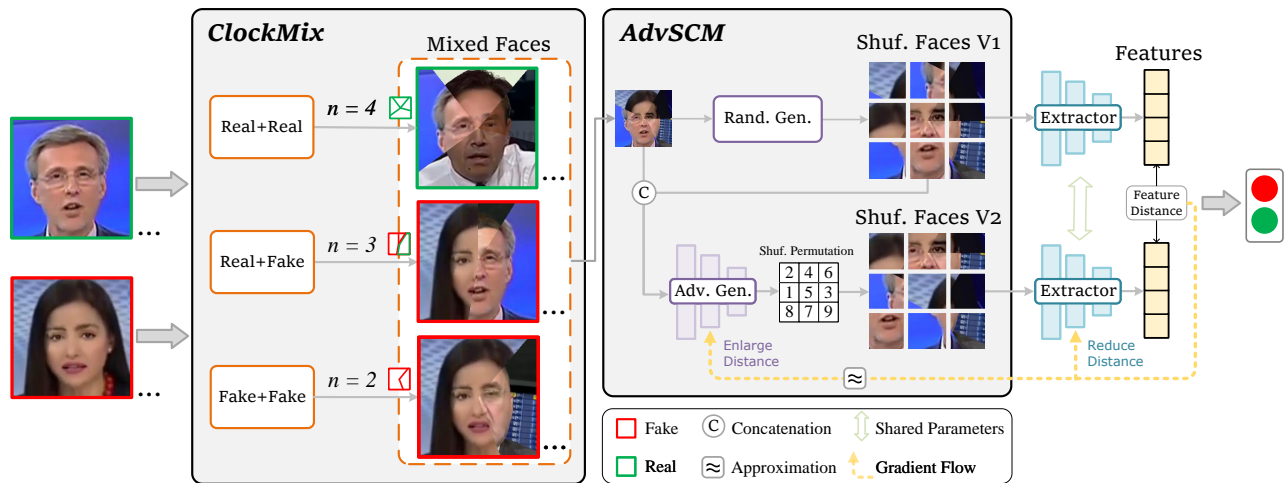


Figure 2: Overall framework of the proposed approach.

2022) proposes to leverage groups of augmented images via dual contrastive learning. Additionally, many strategies introduce diverse data synthesis approaches that are tailored to the deepfake detector. Unlike traditional augmentation, these synthesis methods generate new data from the existing training data and with more defined objectives. Specifically, Face X-ray (Li et al. 2020a) simulates blending artifacts by replacing one pristine face with another pristine face with the nearest landmarks. SLADD (Chen et al. 2022) adopts an adversarial training strategy to select harder forgery artifacts and blend them to pristine faces, obtaining more challenging samples to enhance the sensitivity of the detector. FWA (Li and Lyu 2018) and SBI (Shiohara and Yamasaki 2022) simulated the quality inconsistency by replacing a pristine face with a transformed version of itself, forcing detectors to heighten sensitivity to forged information.

The existing data synthesis methods mixed two paired images with specific regions, which limits the diversity of data mixing. In contrast, our method employs a comprehensive random integration of multiple arbitrary faces with any label, which is beneficial to bias removal.

Proposed Method

Overall Data-level Debiasing Framework

To explicitly remove bias at the data level, we propose a unified framework named ED⁴ with two essential components. Firstly, we propose ClockMix with arbitrary faces to remove content and specific-forgery biases within the samples. Secondly, we introduce the Adversarial Spatial Consistency Module to address the spatial bias. Our method explicitly extends the training distribution with rich compositions of identity, background, manipulation traces, and spatial arrangements, allowing the detector to learn generalizable forgery representations directly and minimize the undesirable effect of the model bias. As the overall architecture shown in Fig. 2, ED⁴ is a plug-and-play module that can be directly implemented into the backbone feature extractor.

ClockMix

To disrupt the shortcut mapping associated with the specific-forgery, background, and identity, we propose ClockMix to randomly integrate faces and backgrounds of arbitrary images. ClockMix performs sector-based mosaicing centered on the face, which is analogous to the rotation of clock hands. Specifically, ClockMix first requires conducting face alignment to ensure that the center of each face is consistently located at the central point of each image according to the face landmarks. Then, we introduce a “clock hand” ray r_h starting at the central point (δ_x, δ_y) and define the angle between r_h and r_{base} as ρ , where r_{base} is a baseline ray starting at the central point toward a random direction. The area in each image swept by r_h upon rotating to ρ will be replaced by the corresponding area from other images within the same mini-batch. To achieve this effect, we calculate a swept-area matrix \mathbf{M} to record the angles between each $r_{(i,j)}$ and the vertical upward-oriented ray r_v , where $r_{(i,j)}$ denotes the ray starting at the central point and passing the pixel located at point (i, j) . Hence, each element in \mathbf{M} can be calculated as:

$$\mathbf{M}(i, j) = \left(\frac{180}{\pi} \arctan 2(\delta_y - i, j - \delta_x) \right) \bmod 360, \quad (1)$$

where $\arctan 2(y, x)$ denotes the angle in radians between the positive x-axis and the ray to the point (x, y) . Considering the angle deviation from r_{base} to r_v , the swept-area matrix for randomly generated r_{base} can be written as:

$$\mathbf{M}_{base} = (\mathbf{M} - \rho_{base}) \bmod 360, \quad (2)$$

where ρ_{base} denotes the deviation angle of r_{base} from r_v . By leveraging \mathbf{M}_{base} , we can conduct ClockMix on arbitrary images \mathbf{I}_a and \mathbf{I}_b to obtain the mixed image \mathbf{I}_{ab} , which can be written as:

$$\begin{aligned} \mathbf{I}_{ab} &= \text{ClockMix}(\mathbf{I}_a, \mathbf{I}_b, \rho_1) \\ &= \mathbf{I}_a \odot (\mathbf{M}_{base} > \rho_1) + \mathbf{I}_b \odot (\mathbf{M}_{base} \leq \rho_1), \end{aligned} \quad (3)$$

where $j \odot k$ yields the value j when the condition k is true, and zero otherwise. ClockMix introduces the simultaneous



Figure 3: Illustration and comparison of ClockMix and previous popular mixing-based methods.

mixing of faces and backgrounds without damaging the fine-grained textures of images including forgery artifacts. Moreover, by aligning with the center of the face, the overall distribution of a single image still maintains the appearance of a normal face, with the correct number and peripheral relationships of facial attributes. Then, to enhance the removal of content and specific-forgery biases, we iteratively conduct ClockMix to enable the mixing of multiple faces and backgrounds into one image. Given \mathbf{I}_{ab} and \mathbf{I}_c , the mixture of three images is made by

$$\mathbf{I}_{abc} = \text{ClockMix}(\mathbf{I}_{ab}, \mathbf{I}_c, \rho_2). \quad (4)$$

To ensure the region from \mathbf{I}_b in \mathbf{I}_{ab} is not completely covered by \mathbf{I}_c , we always let $\rho_2 < \rho_1$. Analogously, ClockMix can sequentially achieve the mixing of n arbitrary images.

Regarding the labels of the mixed images, there are three conditions, that is, *Real+Real*, *Real+Fake*, and *Fake+Fake*. We posit that any mixed image containing forgery should be considered Fake, otherwise, it is deemed as Real. Hence, the output label of the mixed image \mathbf{I}_{ab} is defined by:

$$y_{ab} = 1 - (1 - y_a)(1 - y_b) \quad (5)$$

where $y_a \in \{0, 1\}$ and $y_b \in \{0, 1\}$ are the labels of \mathbf{I}_a and \mathbf{I}_b , respectively. In this paper, we use the label $y = 0$ for real images and $y = 1$ for fake images.

Compared with existing fake synthesizing methods with particular image pair, face region, and label selection (Chen et al. 2022; Dong et al. 2023; Li et al. 2020a), or limited identity and forgery participation (Shiohara and Yamasaki 2022), our ClockMix performs more thorough synthesis with arbitrary images. The deepfake detector is allowed to see mixtures of different identities and backgrounds in both real and fake samples, and the co-occurrence of multiple manipulation clues in one fake image, leading to better removal of the content and specific-forgery bias.

Superiority over existing mixing-based methods. We notice that the proposed ClockMix may share similarities with popular data augmentation strategies that perform pixel mixing, including Mosaic (Bochkovskiy, Wang, and Liao 2020), Mixup (Zhang et al. 2017), and Cutmix (Yun et al. 2019). As shown in Fig. 3, existing strategies are not suitable for debiasing in the deepfake detection task. Specifically, the superiority of ClockMix can be demonstrated by answering two questions: i) What kind of mix is more appropriate for deepfake detection? ii) How to assign the labels for mixed images? For the first question, Mosaic introduces multiple intact faces into one single sample, hence it disrupts the high-level statistical distribution of the training sample and thus confuses the detectors. Mixup can lead to

the overlap of local textures between faces and thus obfuscate the details of forgery artifacts. Cutmix cannot guarantee even mixtures of both face regions and backgrounds from different images simultaneously, thereby reducing its effectiveness in addressing content bias. By contrast, ClockMix conducts sector dividing based on the face center, gaining better control over selecting useful regions and assigning labels. As for the second question, Mosaic is designed for object detection, therefore it is not intuitive to assign a classification label. Mixup and CutMix introduce a mixing label strategy with linear interpolation of

$$\tilde{y}_{ab} = \lambda \cdot y_a + (1 - \lambda) \cdot y_b, \quad (6)$$

with $\lambda \in [0, 1]$. However, in experiments, we observed that linear interpolation of the one-hot labels actually weakens the detector’s ability to identify subtle forgery traces. This is consistent with the basic intuition: an image should be classified as fake even with a small region of manipulated faces. By assigning the hard labels to fake images, ClockMix can greatly increase the sensitivity of the detector to forgery artifacts. More interestingly, we find that referring to the mixture of real images as *real* also plays a critical role in improving the model performance. As ClockMix inevitably introduces unappealing seams with different image pieces, the deepfake detector might be prone to rely on the seaming artifacts for determining authenticity. When we perform mixing on real images with the assignment of real labels, the detector can get rid of the impact of unnatural seams, and meanwhile, distinguish real from fake with improved accuracy. Please refer to the *Ablation Study* for more experimental results and illustrations.

Adversarial Spatial Consistency Module

In this paper, besides content and specific-forgery biases, we have identified a new form of bias, namely *spatial bias*. This bias refers to the detector’s inclination to inertly anticipate observing structural forgery clues at the image center. We believe this issue adversely affects both the effectiveness and robustness of deepfake detection. In terms of effectiveness, inertly focusing on the central area diminishes the sensitivity of the detector to forgery artifacts. Moreover, the anticipation of structural artifacts leads to limited performance in detecting local forgeries. In terms of robustness, it is evident that variations in preprocessing or camera movement are prevalent in practical applications of deepfake detection. Spatial bias compromises the network robustness against such spatial deviation, as detectors primarily concentrate on the image center, yet spatial deviations displace faces and artifacts away from the focal region.

As shown in Fig. 2, we propose the Adversarial Spatial Consistency Module (AdvSCM) to address spatial bias in the extracted feature. The adversarial consistency strategy refers to the generator (enlarging spatial inconsistency) vs. the backbone extractor (reducing feature inconsistency), which closely resembles the generator vs. discriminator in the generative adversarial network. By achieving this, the backbone can learn to extract features that are *spatial-agnostic*, thus avoiding spatial bias. In AdvSCM, we first

introduce spatial shuffle (Chen et al. 2019) as the base operation, which does not undermine the texture and fine-grained information but only produces spatial inconsistency. Then, given an input image \mathbf{I} , two shuffled versions of \mathbf{I} are generated by the random generator $\mathcal{G}_r(\cdot)$ and the adversarial generator $\mathcal{G}_a(\cdot; \theta_a)$, respectively, where θ_a is the learnable parameter in \mathcal{G} . Without learnable parameters, \mathcal{G}_r relocate blocks and reassemble them to obtain the shuffled image $\mathbf{I}_{s1} = \mathcal{G}_r(\mathbf{I})$ with *random* granularity and permutation. In contrast, \mathcal{G}_a is a neural network that inputs the concatenation of \mathbf{I} and \mathbf{I}_{s1} , and outputs a probability metric $\mathbf{m} = \mathcal{G}_a((\mathbf{I}, \mathbf{I}_{s1}); \theta_a) \in \mathbb{R}^{N \times N}$, where N is the number of divided patches for shuffling. \mathbf{m} is then transformed via Hungarian algorithm (Kuhn 1955) to $\hat{\mathbf{m}} \in \{0, 1\}^{N \times N}$, which can be treated as the shuffle permutation for generating \mathbf{I}_{s2} . More details can be found in *Supplementary Material*. Both \mathbf{I}_{s1} and \mathbf{I}_{s2} are then input into the backbone extractor $\mathcal{E}(\cdot; \theta_e)$ to obtain their respective features $\mathbf{F}_{s1}, \mathbf{F}_{s2}$. The optimization target of θ_e is minimizing the distance between \mathbf{F}_{s1} and \mathbf{F}_{s2} , which can be formulated as:

$$\theta'_e = \underset{\theta_e}{\operatorname{argmin}} D, \quad (7)$$

where $D = L_1(\mathbf{F}_{s1}, \mathbf{F}_{s2})$ represents L1 distance between features, θ'_e is the updated parameter, and θ_a should be frozen. Such optimization can be directly implemented via backpropagation. Similarly, θ_a should be optimized for maximizing feature distance:

$$\theta'_a = \underset{\theta_a}{\operatorname{argmax}} D, \quad (8)$$

where θ_e should be frozen. Notably, the gradient flow for optimizing θ_a is broken by non-differentiable operations like sampling and the Hungarian algorithm. Therefore, we approximate the gradient calculation via Reinforce algorithm (Williams 1992):

$$\theta'_a = \theta_a + \frac{\epsilon}{K} \sum_{k=1}^K D \nabla_{\theta_a} \log(p), \quad (9)$$

where K denotes the size of mini-batch, ϵ is the learning rate, and

$$p = \frac{1}{N} \sum_{i=1}^N \sum_{j=1}^N m_{i,j} \hat{m}_{i,j}, \quad (10)$$

where $m_{i,j}$ and $\hat{m}_{i,j}$ refer to the entry located in the i -th row and j -th column of \mathbf{m} and $\hat{\mathbf{m}}$. Both $m_{i,j}$ and $\hat{m}_{i,j}$ can be interpreted as the probability that the patch at the i -th position is shuffled to the j -th position.

By introducing AdvSCM, the adversarial generator learns to predict shuffle configuration that maximizes the spatial inconsistency between generated shuffled images, thus allowing the backbone extractor to more robustly learn spatial-agnostic features via consistency constraints.

Detection Loss

To classify forgeries, the input image \mathbf{I} is processed by the detector and obtains a detection result y' . The ground-truth label y is calculated following Eq. 5 if \mathbf{I} is mixed. Since

ED⁴ requires no modification on the backbone network, the forgery detection loss L_d can be simply measured with the binary cross-entropy loss as

$$L_d(y', y) = -[y \log(y') + (1 - y) \log(1 - y')], \quad (11)$$

which enables the network to identify the forgery images.

Experimental Results

Experimental Setting

Datasets Given that the generalization issue is the major challenge for research, we apply an abundant number of advanced and widely used deepfake datasets in our experiments. FaceForensics++ (FF++) (Rossler et al. 2019) is constructed by four forgery methods including Deepfakes (DF) (DeepFakes. 2021), Face2Face (F2F) (Thies et al. 2016), FaceSwap (FS) (FaceSwap. 2021), and NeuralTextures (NT) (Thies, Zollhöfer, and Nießner 2019). Meanwhile, it includes three different compression quality levels, that is, RAW, High-Quality (HQ), and Low-Quality (LQ). We employ FF++ (HQ) as the training dataset for all experiments in our paper. For cross-dataset evaluations, we introduce Celeb-DF-v1 (CDFv1) (Li et al. 2020b), Celeb-DF-v2 (CDFv2) (Li et al. 2020b), DeepFakeDetection (DFD) (DFD. 2021), and DeepFake Detection Challenge (DFDC) (detection challenge. 2021).

Implementation Details For preprocessing and training, we strictly follow the official code and settings provided by DeepFakeBench (Yan et al. 2023b) to ensure fair comparison. For ClockMix, the number of mixing images is selected from $\{1, 2, 3, 4\}$, and ρ is randomly selected from 45 to 315. Our method takes Xception (Chollet 2017) as the backbone for both adversarial generator and extractor and they are initialized by the parameters pre-trained on ImageNet (Krizhevsky, Sutskever, and Hinton 2012). The Adam optimizer is used with a learning rate of 0.0002, epoch of 10, input size of 256×256 , and batch size of 32. *Frame-level* Area Under Curve (AUC) and Equal Error Rate (EER) (Yan et al. 2023b) are applied as the evaluation metrics of experimental results. All experiments are conducted on one NVIDIA Tesla V100 GPUs.

Cross-dataset Evaluation

In Tab. 1, we provide extensive comparison results with existing state-of-the-art (SOTA) deepfake detectors based on DeepFakeBench (Yan et al. 2023b). Specifically, all methods are trained on FF++ (HQ) and tested on other datasets. The methods in the upper part of the table are within the benchmark with the exact same experimental setting as our method. Hence, we directly *copy* their results from DeepFakeBench. Notably, more SOTA methods are related to our method but are not included in the DeepFakeBench. Considering their implementation details are various (such as SBI (Shiohara and Yamasaki 2022) is trained with FF++ RAW, size of 384, and tested with video-level AUC), we carefully *reproduce* SLADD (Chen et al. 2022) and SBI following their official code within the DeepFakeBench framework, and the results of Liang *et al.* (Liang, Shi, and Deng

Table 1: Cross-dataset evaluations (AUC) from FF++ to CDFv1, CDFv2, DFD and DFDC. C-Avg. denotes the average value of cross-dataset results. The best results are highlighted in **bold**.

Method	Venue	FF++	CDFv1	CDFv2	DFD	DFDC	C-Avg.
Xception (Chollet 2017)	CVPR'17	0.9637	0.7794	0.7365	0.8163	0.7077	0.7600
FWA (Li and Lyu 2018)	CVPRW'18	0.8765	0.7897	0.6680	0.7403	0.6132	0.7028
Meso4 (Afchar et al. 2018)	WIFS'18	0.6077	0.7358	0.6091	0.5481	0.5560	0.6123
Capsule (Nguyen, Yamagishi, and Echizen 2019)	ICASSP'19	0.8421	0.7909	0.7472	0.6841	0.6465	0.7172
EfficientNetB4 (Tan and Le 2019)	ICML'19	0.9567	0.7909	0.7487	0.8148	0.6955	0.7625
CNN-Aug (Wang et al. 2020)	CVPR'20	0.8493	0.7420	0.7027	0.6464	0.6361	0.6818
X-ray (Li et al. 2020a)	CVPR'20	0.9592	0.7093	0.6786	0.7655	0.6326	0.6965
FFD (Dang et al. 2020)	CVPR'20	0.9624	0.7840	0.7435	0.8024	0.7029	0.7582
F3Net (Qian et al. 2020)	ECCV'20	0.9635	0.7769	0.7352	0.7975	0.7021	0.7530
SPSL (Liu et al. 2021)	CVPR'21	0.9610	0.8150	0.7650	0.8122	0.7040	0.7741
SRM (Luo et al. 2021)	CVPR'21	0.9576	0.7926	0.7552	0.8120	0.6995	0.7648
CORE (Ni et al. 2022)	CVPRW'22	0.9638	0.7798	0.7428	0.8018	0.7049	0.7573
Recce (Cao et al. 2022)	CVPR'22	0.9621	0.7677	0.7319	0.8119	0.7133	0.7562
UIA-VIT (Zhuang et al. 2022)	ECCV'22	0.9655	0.7925	0.8002	0.8279	0.7038	0.7811
IID (Huang et al. 2023)	CVPR'23	0.9743	0.7578	0.7687	0.7935	0.6951	0.7538
UCF (Yan et al. 2023a)	ICCV'23	0.9705	0.7793	0.7527	0.8074	0.7191	0.7646
Liang <i>et al.</i> (Liang, Shi, and Deng 2022)	ECCV'22	-	0.706	-	0.829	0.700	-
SLADD (Chen et al. 2022)	CVPR'22	0.9691	0.8015	0.7403	0.8089	0.7170	0.7669
SBI (Shiohara and Yamasaki 2022)	CVPR'22	0.9747	0.8371	0.7911	0.8112	0.7275	0.7917
LSDA (Yan et al. 2024)	CVPR'24	-	0.867	0.830	0.880	0.736	0.828
Ours	-	0.9806	0.8871	0.8394	0.8765	0.7427	0.8364

Table 2: The impact of ClockMix (CM) and Adversarial Spatial Consistency Module (AdvSCM).

Method	DFD		CDFv2		DFDC	
	AUC	EER	AUC	EER	AUC	EER
Baseline	0.7994	0.2738	0.7454	0.3209	0.7089	0.3621
w/o CM	0.8336	0.2280	0.7802	0.2907	0.7105	0.3517
w/o AdvSCM	0.8200	0.2499	0.7712	0.3143	0.7296	0.3327
Ours	0.8765	0.1939	0.8394	0.2283	0.7427	0.3048

2022) are reproduced by (Yan et al. 2023a). LSDA (Yan et al. 2024) is the new SOTA based on DeepFakeBench, therefore we directly copy the results from their paper.

It can be observed that our method consistently outperforms the earlier deepfake detectors based on data synthesis techniques (*i.e.*, FWA, X-ray, SLADD, and SBI) across all evaluated datasets. Meanwhile, compared with the implicit disentanglement methods (*i.e.*, Liang *et al.* and UCF), our method also exhibits superior effectiveness. More cross-dataset results for our method can be found in *Supplementary Material*. These results demonstrate the superiority of the proposed explicit data-level debiasing approach over previous SOTA methods.

Ablation Study

Impact of Different Proposed Components In Tab. 2, we assess the effectiveness of each proposed component. The detector trained without all proposed components is denoted by Baseline. The results on all evaluated datasets and metrics demonstrate that each component essentially contributes to

Table 3: Comparison of different mixing and label-assignment strategies. HL indicates assigning hard labels with Eq. (5), and SL denotes calculating soft labels with Eq. (6). MRF denotes assigning the mixture of real images with the *fake* label.

Method	DFD		CDFv2		DFDC	
	AUC	EER	AUC	EER	AUC	EER
CM-MRF	0.6061	0.4571	0.5419	0.4833	0.5351	0.4877
Mosaic-HL	0.7101	0.3479	0.5939	0.4638	0.5714	0.4312
Mosaic-SL	0.7915	0.2678	0.7549	0.3101	0.6792	0.3795
CutMix-HL	0.8399	0.2124	0.7862	0.2868	0.7231	0.3471
CutMix-SL	0.7534	0.2910	0.7357	0.3279	0.6322	0.4301
Mixup-HL	0.8167	0.2518	0.7575	0.3023	0.6959	0.3601
Mixup-SL	0.8013	0.2802	0.7464	0.3173	0.7009	0.3595
CM-SL	0.8104	0.2593	0.7953	0.2799	0.7191	0.3584
CM-HL(Ours)	0.8765	0.1939	0.8394	0.2283	0.7427	0.3048

the effectiveness of our method.

Configurations of ClockMix To demonstrate the superiority of the proposed ClockMix, we replace ClockMix with traditional data mixing augmentations, that is, Mosaic (Bochkovskiy, Wang, and Liao 2020), Mixup (Zhang et al. 2017) and CutMix (Yun et al. 2019). We also investigate the influences of label-assigning strategies, including Hard Label (HL), Soft Label (SL), and assigning the Mixture of Real images with the Fake label (MRF). In Tab. 3, we first observe that MRF fundamentally destroys the detector’s ability to justify forgery clues. This can be attributed to all images with ClockMix being assigned with Fake labels,

Table 4: Effectiveness of the proposed adversarial strategy compared with random strategies.

Method	DFD		CDFv2		DFDC	
	AUC	EER	AUC	EER	AUC	EER
RS	0.8279	0.2367	0.7839	0.2917	0.7304	0.3209
RS+C	0.8795	0.1892	0.8033	0.2709	0.7212	0.3434
AdvSCM (Ours)	0.8765	0.1939	0.8394	0.2283	0.7427	0.3048

Table 5: Results (AUC) of adding ED⁴ to existing deepfake detection methods for plug-and-play effectiveness.

Method	DFD	CDFv2	DFDC
Effnb4	0.8004	0.7531	0.6848
Effnb4 + ED ⁴	0.8550 (↑ 7%)	0.8129 (↑ 8%)	0.7214 (↑ 5%)
Capsule	0.7622	0.7062	0.6744
Capsule + ED ⁴	0.8183 (↑ 7%)	0.7942 (↑ 12%)	0.7243 (↑ 7%)
SPSL	0.8151	0.7499	0.6859
SPSL + ED ⁴	0.8656 (↑ 6%)	0.8115 (↑ 8%)	0.7361 (↑ 7%)

hence the detector mistakenly takes the ClockMix splicing patterns as the indicator of forgery. The proposed ClockMix-HL significantly outperforms all ablation variants in performance. Image with Mosaic cannot be applied with HL considering the intact information is preserved for each mixed face. Meanwhile, it can be observed that SL severely undermines the effectiveness of CutMix and ClockMix by categorizing the Real+Fake images under an uncertain label, which reduces the confidence in determining fake images with minor forgery artifacts. Since applying Mixup renders the details of forgery artifacts, both HL and SL versions of Mixup compromise the effectiveness of the deepfake detector.

Effect of Adversarial Spatial Consistency Module To validate the effectiveness of the proposed adversarial consistency strategy, we design two ablation variants: 1) Random Shuffle (RS), where we only deploy random shuffle to the image, and take the shuffled image as the training input. 2) Random Shuffle Consistency (RS+C), where we generate two random shuffle versions of an image, and apply Eq. (7) to encourage their consistency without using Eq. (9) for the adversarial strategy. Tab. 4 shows that RS+C exhibits slightly superior effectiveness on the DFD dataset. However, it cannot stably perform best in different cross-dataset settings. In contrast, deploying AdvSCM enhances the overall cross-dataset generalization ability of deepfake detection.

Plug-and-Play with Previous Deepfake Detectors

Considering our debiasing method is explicitly applied at the data level, it can be directly implemented to existing SOTA methods for deepfake detection. Therefore, we reproduce EfficientNetB4 (Effnb4) (Tan and Le 2019), SPSL (Liu et al. 2021), and Capsule (Nguyen, Yamagishi, and Echizen 2019) and then adding ED⁴ to them. Tab. 5 shows that with the additive implementation of ED⁴, all detectors exhibit significant enhancements in performance. This substantiates that

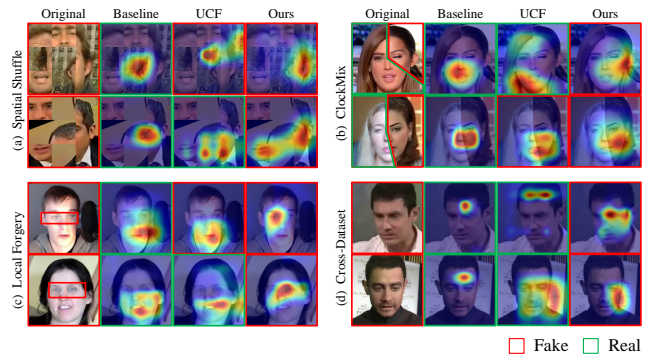


Figure 4: Comparisons of CAM for different methods.

our method is plug-and-play that can be conveniently applied to other methods to enhance their effectiveness.

Qualitative Results

In this section, we visualize the Class Activation Map (CAM) via Grad-CAM++ (Chattopadhyay et al. 2018) to discuss the focal regions of different detectors. UCF (Yan et al. 2023a) is the most advanced method that addresses model bias by feature disentanglement via implicit network design. In Fig. 4, we provide the CAM of images with four different conditions. Specifically, Spatial Shuffle (Fig. 4 (a)) and ClockMix (Fig. 4 (b)) are operations introduced by our method. Local Forgery (Fig. 4 (c)) is achieved by replacing eyes in the real faces with the fake ones following (Chen et al. 2022). Images in Cross-Dataset (Fig. 4 (d)) are from CDFv1 while detectors are trained on FF++.

Suffering from spatial bias, the Baseline is inertly focusing on the relatively central regions despite the facial regions being relocated or locally replaced. UCF can perceive forgery clues in a wider region of the image center (the 2nd rows in Fig. 4 (a) and (c)), but it also struggles to precisely locate the forgery artifacts (Fig. 4 (b) and the 1st rows in Fig. 4 (a) and (c)). Conversely, our method can adaptively focus on the local forgery artifacts at diverse image locations. Fig. 4 (d) indicates the challenges for the existing methods to detect the common artifacts in cross-dataset settings. Namely, the Baseline fails to perceive forgery, while UCF may overlook the actual forgery regions (the 2nd row in Fig. 4 (d)). Conversely, our method exhibits superior sensitivity to the cross-dataset common forgery artifacts.

Conclusion

In this paper, we improve the deepfake detector’s generalizability from the debiasing perspective. Firstly, besides content and specific-forgery biases, we reveal a new form of model bias termed spatial bias. That is, the deepfake detector consistently anticipates observing structural forgery clues at the image center. Then, we propose Explicit Data-level Debiasing for Deepfake Detection (ED⁴), which is a unified framework to address the aforementioned three biases. Specifically, we propose ClockMix with multiple arbitrary faces to eliminate content and specific-forgery biases. For the spatial bias, we introduce the Adversarial Spatial

Consistency Module (AdvSCM) that forces the backbone to extract spatial-agnostic features. Considering the improved effectiveness and plug-and-play convenience, ED⁴ can be treated as a superior alternative to implicit disengagement by network design. Experiments demonstrate the promising performance of our method.

References

- Afchar, D.; Nozick, V.; Yamagishi, J.; and Echizen, I. 2018. Mesonet: a compact facial video forgery detection network. In *IEEE International Workshop on Information Forensics and Security*, 1–7. IEEE.
- Bai, W.; Liu, Y.; Zhang, Z.; Li, B.; and Hu, W. 2023. AUNet: Learning Relations Between Action Units for Face Forgery Detection. In *CVPR*, 24709–24719.
- Bochkovskiy, A.; Wang, C.-Y.; and Liao, H.-Y. M. 2020. Yolov4: Optimal speed and accuracy of object detection. *arXiv preprint arXiv:2004.10934*.
- Cao, J.; Ma, C.; Yao, T.; Chen, S.; Ding, S.; and Yang, X. 2022. End-to-end reconstruction-classification learning for face forgery detection. In *CVPR*, 4113–4122.
- Chattopadhyay, A.; Sarkar, A.; Howlader, P.; and Balasubramanian, V. N. 2018. Grad-cam++: Generalized gradient-based visual explanations for deep convolutional networks. In *WACV*, 839–847. IEEE.
- Chen, L.; Zhang, Y.; Song, Y.; Liu, L.; and Wang, J. 2022. Self-supervised learning of adversarial example: Towards good generalizations for deepfake detection. In *CVPR*, 18710–18719.
- Chen, Y.; Bai, Y.; Zhang, W.; and Mei, T. 2019. Destruction and construction learning for fine-grained image recognition. In *CVPR*, 5157–5166.
- Chollet, F. 2017. Xception: Deep learning with depthwise separable convolutions. In *CVPR*, 1251–1258.
- Dang, H.; Liu, F.; Stehouwer, J.; Liu, X.; and Jain, A. K. 2020. On the detection of digital face manipulation. In *CVPR*.
- DeepFakes. 2021. www.github.com/deepfakes/faceswap Accessed 2021-04-24.
- detection challenge., D. 2021. <https://www.kaggle.com/c/deepfake-detection-challenge> Accessed 2021-04-24.
- DFD. 2021. <https://ai.googleblog.com/2019/09/contributing-data-to-deepfake-detection.html> Accessed 2021-04-24.
- Dong, S.; Wang, J.; Ji, R.; Liang, J.; Fan, H.; and Ge, Z. 2023. Implicit Identity Leakage: The Stumbling Block to Improving Deepfake Detection Generalization. In *CVPR*, 3994–4004.
- FaceSwap. 2021. www.github.com/MarekKowalski/FaceSwap Accessed 2021-04-24.
- Haliassos, A.; Vougioukas, K.; Petridis, S.; and Pantic, M. 2021. Lips Don't Lie: A Generalisable and Robust Approach To Face Forgery Detection. In *CVPR*.
- Huang, B.; Wang, Z.; Yang, J.; Ai, J.; Zou, Q.; Wang, Q.; and Ye, D. 2023. Implicit Identity Driven Deepfake Face Swapping Detection. In *CVPR*, 4490–4499.
- Krizhevsky, A.; Sutskever, I.; and Hinton, G. E. 2012. Imagenet classification with deep convolutional neural networks. *NeurIPS*, 25.
- Kuhn, H. W. 1955. The Hungarian method for the assignment problem. *Naval research logistics quarterly*, 2(1-2): 83–97.
- Li, L.; Bao, J.; Zhang, T.; Yang, H.; Chen, D.; Wen, F.; and Guo, B. 2020a. Face x-ray for more general face forgery detection. In *CVPR*.
- Li, Y.; and Lyu, S. 2018. Exposing deepfake videos by detecting face warping artifacts. *arXiv preprint arXiv:1811.00656*.
- Li, Y.; Yang, X.; Sun, P.; Qi, H.; and Lyu, S. 2020b. Celebdf: A new dataset for deepfake forensics. In *CVPR*.
- Liang, J.; Shi, H.; and Deng, W. 2022. Exploring Disentangled Content Information for Face Forgery Detection. In *ECCV*, 128–145. Springer.
- Liu, H.; Li, X.; Zhou, W.; Chen, Y.; He, Y.; Xue, H.; Zhang, W.; and Yu, N. 2021. Spatial-phase shallow learning: re-thinking face forgery detection in frequency domain. In *CVPR*, 772–781.
- Luo, Y.; Zhang, Y.; Yan, J.; and Liu, W. 2021. Generalizing Face Forgery Detection with High-frequency Features. In *CVPR*.
- Nguyen, H. H.; Yamagishi, J.; and Echizen, I. 2019. Capsule-forensics: Using capsule networks to detect forged images and videos. In *ICASSP*, 2307–2311. IEEE.
- Ni, Y.; Meng, D.; Yu, C.; Quan, C.; Ren, D.; and Zhao, Y. 2022. CORE: Consistent Representation Learning for Face Forgery Detection. In *CVPR Workshop*, 12–21.
- Qian, Y.; Yin, G.; Sheng, L.; Chen, Z.; and Shao, J. 2020. Thinking in frequency: Face forgery detection by mining frequency-aware clues. In *ECCV*, 86–103. Springer.
- Rossler, A.; Cozzolino, D.; Verdoliva, L.; Riess, C.; Thies, J.; and Nießner, M. 2019. Faceforensics++: Learning to detect manipulated facial images. In *ICCV*, 1–11.
- Shiohara, K.; and Yamasaki, T. 2022. Detecting deepfakes with self-blended images. In *CVPR*, 18720–18729.
- Sun, K.; Yao, T.; Chen, S.; Ding, S.; Li, J.; and Ji, R. 2022. Dual contrastive learning for general face forgery detection. In *AAAI*, volume 36, 2316–2324.
- Tan, M.; and Le, Q. 2019. Efficientnet: Rethinking model scaling for convolutional neural networks. In *ICML*, 6105–6114. PMLR.
- Thies, J.; Zollhöfer, M.; and Nießner, M. 2019. Deferred neural rendering: Image synthesis using neural textures. *TOG*, 38(4): 1–12.
- Thies, J.; Zollhofer, M.; Stamminger, M.; Theobalt, C.; and Nießner, M. 2016. Face2face: Real-time face capture and reenactment of rgb videos. In *CVPR*, 2387–2395.
- Wang, C.; and Deng, W. 2021. Representative forgery mining for fake face detection. In *CVPR*, 14923–14932.
- Wang, S.-Y.; Wang, O.; Zhang, R.; Owens, A.; and Efros, A. A. 2020. CNN-generated images are surprisingly easy to spot... for now. In *CVPR*, 8695–8704.

Williams, R. J. 1992. Simple statistical gradient-following algorithms for connectionist reinforcement learning. *ML*, 8: 229–256.

Yan, Z.; Luo, Y.; Lyu, S.; Liu, Q.; and Wu, B. 2024. Transcending forgery specificity with latent space augmentation for generalizable deepfake detection. In *CVPR*, 8984–8994.

Yan, Z.; Zhang, Y.; Fan, Y.; and Wu, B. 2023a. UCF: Uncovering Common Features for Generalizable Deepfake Detection. *ICCV*.

Yan, Z.; Zhang, Y.; Yuan, X.; Lyu, S.; and Wu, B. 2023b. Deepfakebench: A comprehensive benchmark of deepfake detection. *arXiv preprint arXiv:2307.01426*.

Yun, S.; Han, D.; Oh, S. J.; Chun, S.; Choe, J.; and Yoo, Y. 2019. Cutmix: Regularization strategy to train strong classifiers with localizable features. In *CVPR*, 6023–6032.

Zhang, H.; Cisse, M.; Dauphin, Y. N.; and Lopez-Paz, D. 2017. mixup: Beyond empirical risk minimization. *arXiv preprint arXiv:1710.09412*.

Zhong, Z.; Zheng, L.; Kang, G.; Li, S.; and Yang, Y. 2020. Random erasing data augmentation. In *AAAI*, volume 34, 13001–13008.

Zhuang, W.; Chu, Q.; Tan, Z.; Liu, Q.; Yuan, H.; Miao, C.; Luo, Z.; and Yu, N. 2022. UIA-ViT: Unsupervised inconsistency-aware method based on vision transformer for face forgery detection. In *ECCV*, 391–407. Springer.

Supplementary Materials

More Implementation Details

Detailed Experimental Setting

Here, we provide the implementation configuration we applied for the experiments of the main paper. To ensure fair comparisons, all methods present in our paper follow the same configurations from DeepfakeBench (Yan et al. 2023b) as we provided below. Dlib (?) is used for face extraction and alignment with a cropping margin of 15%. 32 frames are extracted from each video and all frames are cropped to the size of 256×256 . For training, traditional data augmentations are deployed including rotating, Gaussian noise, saturation adjusting, and quality adjusting.

Detailed Implementations of the Adversarial Generator

Due to length limitations, we did not provide a detailed introduction to the proposed adversarial generator in the main manuscript. Here, we comprehensively discuss the architectural details of the adversarial generator and the rationale for applying linear programming to the probability metric m via the Hungarian algorithm. Firstly, our adversarial generator is based on an Xception backbone. Given a granularity g , the number of divided patches is $N = g^2$, and hence the shape of the output possibility metric \mathbf{m} is $N \times N$, where the first N refers to the number of patches in the shuffled image, the second one refers to the possible shuffled location of patches. Such an effect can be easily achieved by deploying a linear layer that outputs $N \times N$ after the Xception backbone and then reshaping the output.

However, directly using \mathbf{m} to guide the shuffling of images could be problematic. Specifically, each region should be assigned to a unique patch, that is, the predicted region index for each patch must be distinct. In fact, this mutual exclusivity of indices aligns with solving polynomials, except we are maximizing polynomials instead of minimizing them, which could be easily transformed by adding a minus sign to \mathbf{m} . Therefore, the problem can be formulated as:

$$\text{minimize } \sum_{i=1}^N \sum_{j=1}^N -m_{i,j} \hat{m}_{i,j}, \quad (12)$$

where $x_{i,j} \in \{0, 1\}$ and

$$\prod_{i=1}^N \sum_{j=1}^N \hat{m}_{i,j} = 1, \prod_{i=1}^N \sum_{i=1}^N \hat{m}_{i,j} = 1. \quad (13)$$

Subsequently, we utilize the Hungarian algorithm to solve this polynomial and hence convert \mathbf{m} into $\hat{\mathbf{m}}$. Then, the max indices in each row of $\hat{\mathbf{m}}$ could be directly used as the permutation that can guide the shuffling. We provide a visualized example for a better illustration of the aforementioned process in Fig 5.

Robustness Evaluation

Robustness Against Unseen Perturbations

As shown in Fig. 7, we introduce block-wise and blur for the robustness evaluation against unseen perturbations. To

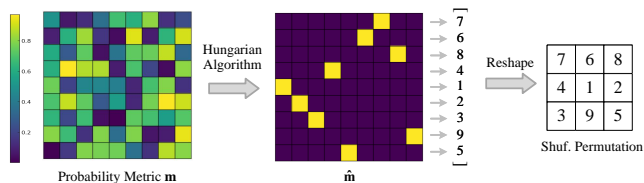


Figure 5: Visualized example of transforming generator output to shuffle permutation.

comprehensively investigate the robustness, we set the intensity of perturbations to gradually increase. Obviously, our method exhibits superior robustness due to the improved reception of forgery clues.

Robustness Against Spatial Deviations

We provide a prediction stability study to investigate the robustness against spatial deviation. Specifically, we quantify the variation in prediction confidence for each image after applying the spatial deviation and subsequently depict these variations as a histogram in Fig. 7. Mathematically, the deviation value at each image can be written as $|\mathcal{N}(\mathbf{I}) - \mathcal{N}(\mathcal{T}_s(\mathbf{I}))|$, where $\mathcal{N}(\cdot)$ is the detection network, \mathbf{I} is the original image, and \mathcal{T}_s is one of the spatial transforming operation. A larger variation indicates a worse detection stability. For the baseline detector, a considerable number of detection results suffer from the spatial deviation. Especially for Crop, over one-third of the variations exceed 0.5, indicating a notable number of detection results are reversed to the opposite after spatial deviation. In contrast, with the help of AdvSCM, our detector can maintain strong robustness against different spatial deviations.

More Ablation Study

Comparison with More Augmentation Methods for Spatial Bias

As shown in Tab. 6, we introduce three approaches to replace Shuffle that may contribute to spatial bias removal: 1) Grid-Mask (?), which is a widely-used augmentation that randomly masks a certain ratio of images. 2) AttrMask, which can mask out certain facial attributes guided by the facial landmarks. 3) RandomCrop, which alters the relative location of faces in the images. The w/o AdvSCM can be treated

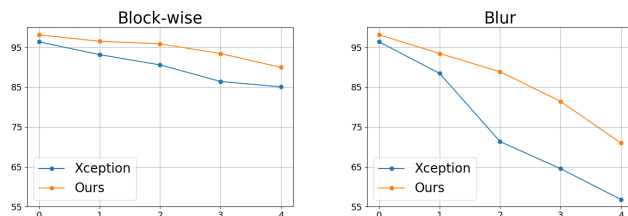


Figure 6: Robustness on Unseen Perturbations

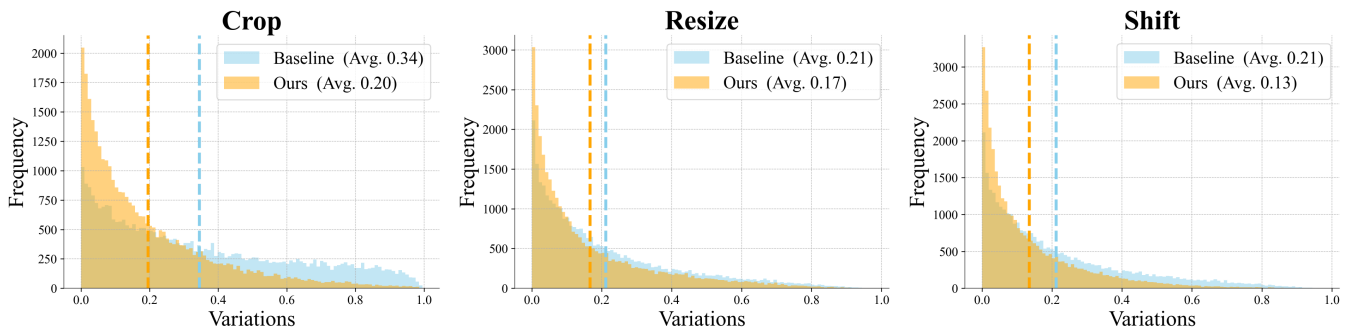


Figure 7: Robustness against spatial deviations. "Variations" indicates the variation of prediction scores when applying different spatial transformations. The dotted lines represent the average variation

Table 6: Comparison with more augmentation methods for spatial bias. Local represents the introduction of local forgery. Region denotes introducing region variations. Info-I denotes Informative pixel Integrity.

Method	Local	Region	Info-I	DFD	CDFv2	DFDC	Avg.
w/o AdvSCM (Baseline)			✓	0.8200	0.7712	0.7296	0.7736
GridMask		✓		0.8408	0.7838	0.7312	0.7853
AttrMask		✓		0.8005	0.7139	0.6759	0.7301
RandomCrop	✓			0.8415	0.8150	0.7235	0.7933
Shuffle	✓	✓	✓	0.8765	0.8394	0.7427	0.8195

Table 7: Investigation for mixing images with different labels. Avg. denotes the Average performance in the cross-dataset evaluation.

Method	DFD	CDFv2	DFDC	Avg.
Baseline	0.7994	0.7454	0.7089	0.7512
w/o Real+Real	0.7177	0.6959	0.6361	0.6832
w/o Real+Fake	0.8481	0.8045	0.7255	0.7927
w/o Fake+Fake	0.8560	0.7931	0.7247	0.7913
Ours	0.8765	0.8394	0.7427	0.8195

as the baseline for which no spatial transformation is deployed. The masking-based methods can break the structural forgery into local ones, but cannot improve the model sensitivity to artifacts at arbitrary regions. While RandomCrop can alter the forgery location to some extent but still maintain the forgery structure. Meanwhile, since masking and cropping lead to the reduction of informative pixels, the performances achieved by these methods are not as pronounced as our S-Shuffle. Especially for AttrMask, despite masking certain facial attributes that may enhance the model sensitivity to local forgery, it significantly reduces the pixels that likely contain forgery information and thus leads to performance degradation. Moreover, this information reduction further leads to inherent inconsistency in extracted features, thereby rendering the employment of Consistency Loss inappropriate. In contrast, deploying Shuffle can uniformly address spatial bias while maintaining informative

pixel integrity. Therefore, we use Shuffle as the basic spatial operation to construct the proposed adversarial spatial consistency module.

The Effectiveness of Conducting ClockMix on Arbitrary Images

To investigate the influence of conducting ClockMix on arbitrary images, we perform an ablation study with three ablation variants, that is, w/o Real+Real, w/o Real+Fake, and w/o Fake+Fake. As shown in Tab. 7, w/o Real+Real will undermine the performance by indulging the detector to take the seaming patterns as fake. Such a result is similar to the "mixture of real images with the fake label (MRF)" that we present in the main paper except the degradation is slighter. Overall, the lack of any label combination in ClockMix can lead to considerable performance degradation, which indicates the superiority of mixing arbitrary images over existing label-specific and image-specific synthesis methods.

More Cross-dataset Evaluations

In this section, we provide results of our method on **seven** more datasets, including WildDeepfake (?) (WDF), FakeAVCeleb (?) (FAVC), {E4S (?), BlendFace (?), UniFace (?), DeepfaceLab (?) (DFL)} from DF40 (?), and {DiffSwap (?)} from DiffusionFace (?). Considering most baseline methods from DeepfakeBench (Yan et al. 2023b) have not been reproduced on these advanced datasets, we carefully reproduce EfficientNet (Tan and Le 2019), Xception (Chollet 2017), SPSL (Liu et al. 2021), and UCF (Yan et al. 2023a) and evaluate them on these datasets for compar-

Table 8: Cross-dataset Evaluations on more various datasets. The metric is frame-level AUC and all models are trained on FF++ (Rossler et al. 2019).

Methods	WDF	FAVC	DiffSwap	E4S	BlendFace	UniFace	DFL	Avg.
EfficientNet	0.7275	0.8404	0.7956	0.6514	0.7813	0.7775	0.7347	0.7583
Xception	0.7705	0.8681	0.8110	0.6554	0.7911	0.8282	0.7199	0.7777
SPSL	0.7023	0.7689	0.7784	0.5987	0.6936	0.6915	0.6548	0.6983
UCF	0.7738	0.8631	0.8511	0.6916	0.7850	0.7867	0.7433	0.7849
Ours	0.7682	0.8879	0.8781	0.7201	0.8511	0.8280	0.7794	0.8161

ison. As shown in Tab. 8, it can be observed that our methods can be generalized to various datasets with superior effectiveness.